

## Parallel Analog Computing Based on a $2 \times 2$ Multiple-Input Multiple-Output Metasurface Processor With Asymmetric Response

Amirhossein Babaee<sup>1</sup>, Ali Momeni,<sup>2</sup> Ali Abdolali,<sup>1,\*</sup> and Romain Fleury<sup>2</sup>

<sup>1</sup>*Applied Electromagnetic Laboratory, School of Electrical Engineering, Iran University of Science and Technology, Tehran, Iran*

<sup>2</sup>*Laboratory of Wave Engineering, Swiss Federal Institute of Technology in Lausanne (EPFL), CH-1015 Lausanne, Switzerland*

(Received 16 April 2020; revised 4 December 2020; accepted 25 February 2021; published 7 April 2021)

We present a polarization-insensitive metasurface processor to perform spatial asymmetric filtering of an incident beam, thereby allowing for real-time parallel analog processing. To enable massive parallel processing, we introduce a multiple-input multiple-output (MIMO) computational metasurface with asymmetric response that can perform spatial differentiation on two distinct input signals regardless of their polarization. In our scenario, two distinct signals set in  $x$  and  $y$  directions, parallel and perpendicular to the incident plane, illuminate simultaneously the metasurface processor, and the resulting differentiated signals are separated from each other via appropriate spatial low-pass filters. By leveraging generalized sheet transition conditions and surface susceptibility tensors, we design an asymmetric meta-atom augmented with normal susceptibilities to reach asymmetric response at normal beam illumination. Proof-of-principle simulations are also reported along with the successful realization of signal processing functions. The proposed metasurface overcomes major shortcomings imposed by previous studies, such as large architectures arising from the need for additional subblocks, slow responses, and, most importantly, supporting only a single input with a given polarization. Our results set the path for future developments of material-based analog computing using efficient and easy-to-fabricate MIMO processors for compact, fast, and integrable computing elements without any Fourier lens.

DOI: 10.1103/PhysRevApplied.15.044015

### I. INTRODUCTION

With the expeditious development of technology in today's communications systems, signal and image processing has gained a lot of attention in the past decade [1–3]. The idea of signal processing by analog computing has been known for a long time, but in the late 20th century, when the digital revolution began, digital computation sat in place of analog computation. Although it was a huge breakthrough, these digital systems suffer from serious restrictions such as data conversion loss and operational speed [4]. Analog solutions therefore emerged again and proved to be advantageous for specific tasks, for example the processing of large-size images [5,6]. Optical signal processing, in particular, largely overcomes the serious limitations of digital systems in terms of speed and power consumption [6]. Therefore, designing fast, integrated, and ultralow-power-consumption optical devices with high throughput is one of the key necessities for developing today's modern optical analog processing, and

moving towards commercial applications with real-time performance.

Spatial optical analog computing based on computational metamaterials is generally based on two major methods: Green's function (GF) method and metamaterial surfaces (metasurfaces), with two additional sub-blocks to apply Fourier and inverse Fourier transforms [7–9]. Both approaches, however, suffer from the large final size of the system [5,7,8]. Over the past few years, in order to sidestep the drawbacks associated with the Fourier transform sub-blocks, optical analog computing based on a single metasurface has attracted particular attention as artificial real-time and high-throughput thin-film processing. This allows migrating from free-space and bulky systems into conceptually subwavelength-sized meta-atoms to perform mathematical operations [10–27]. Metasurfaces that efficiently manipulate the optical wave in the spatial domain are synthesized via several approaches such as generalized sheet transition conditions (GSTCs) and susceptibility tensors, which provide an insightful vision for the engineering of meta-atoms with specific angular scattering properties [13,15,28–32]. Due to their benefits in terms of low profile, low sensitivity to absorption

\*abdolali@iust.ac.ir

losses, and ease of fabrication, metasurfaces are interesting practical alternatives for bulky solutions, especially when it comes to applications including tunable/broadband scattering manipulation [33–44] or antenna engineering [45–47].

In order to be relevant to the widest possible class of signal processing operations, it is important that designed optical systems can operate filtering operations on multiple inputs, especially to develop massive parallel processing schemes. Recently, some proposals have theoretically introduced parallel signal processing for inputs at different angles or two orthogonal polarizations [13,15,16]. Although numerous efforts have been made to expand the functionalities of wave-based signal processing systems, a solution allowing for parallel signal processing without the stringent requirements of working at different incidence angles or given polarization states has not yet been proposed. In addition, another resurgent challenge is creating a metasurface processor with an asymmetric response with respect to transverse momentum, namely one that distinguishes between  $-k_t$  and  $k_t$  components of normally incident beams. Such odd transfer functions (TFs) are needed for first-order differentiation and edge detection [48–50]. Indeed, among all mathematical operations, spatial differentiation is a fundamental mathematical operation used in many fields of science and engineering, and it is appealing for real-time image processing such as image sharpening and edge-based segmentation, with broad applications ranging from microscopy and medical imaging to industrial inspection and object detection [49].

In this paper, we design a multiple-input multiple-output (MIMO) computational metasurface for performing parallel analog processing with odd TF on the transmission operational mode at normal beam illumination. We propose and demonstrate a real-time parallel polarization-insensitive metasurface processor that can act as first-order differentiation operator for both TE and TM states. Systematically speaking, here, we propose a  $2 \times 2$  MIMO first-order differentiation processor for both orthogonal polarizations. The inputs and outputs correspond to different beam amplitude variations along orthogonal directions for a given polarization and angle. Using GSTCs and susceptibility tensors, we show that the presence of normal susceptibility components is required for breaking the even transmission symmetry at normal illumination. Additionally, based on relationships between the structural symmetries of the meta-atoms and the corresponding symmetries of their angular scattering response, we propose a simple meta-atom with geometric symmetry with respect to the  $x = y$  line, which enables first-order derivation for both input signals and both orthogonal polarizations. The waves transmitted through the metasurface processor are then processed by simple spatial low-pass filters (SLPFs) in order to extract and separate the output signal with

$x$  variations from the one with  $y$  variations. In order to demonstrate the concept, we provide a numerical example based on arbitrary input signals. The synthesized metasurface paves a path towards the implementation of MIMO spatial analog mathematical systems to accelerate optical signal and image processing routines.

## II. GSTC AND META-ATOM DESIGN

The general concept of wave-based MIMO signal processing for normally incident beams is summarized in Fig. 1. We consider the  $2 \times 2$  MIMO differentiation processor for two momentous reasons. Firstly, first-order differentiation operation is one of the fundamental operations in mathematics that has several applications in engineering especially for edge detection [13,14,19,33]. Secondly, this basic operation requires a TF with odd phase response with respect to the transverse wave number  $k_x$  that makes designing such an asymmetric TF more complicated in comparison with the symmetric one. It is clear that the  $2 \times 2$  MIMO processor can be considered for other TFs including symmetric and asymmetric types. It means that if we want to have a  $2 \times 2$  MIMO metasurface processor for other operations, we should realize the meta-atom according to the corresponding TF. We consider the case of a  $2 \times 2$  MIMO first-order differentiation processor. Two distinct input signals,  $\psi_{\text{inc},1}^{\text{TE/TM}}(x)$  and  $\psi_{\text{inc},2}^{\text{TE/TM}}(y)$ , with  $x$  and  $y$  variations, illuminate simultaneously the metasurface processor for a given (TE or TM) polarization. By properly designing the metasurface processor, the transmitted waves possess the same polarization as the input and contain a sum of their first-order differentiated signals. We then utilize two SLPFs, along  $k_x$  and  $k_y$ , to extract the desired output signals, namely  $(d/dx)\psi_{\text{inc},1}^{\text{TE/TM}}(x)$  and  $(d/dy)\psi_{\text{inc},2}^{\text{TE/TM}}(y)$ . Theoretically speaking, we start from a reciprocal passive metasurface processor consisting of a periodic and homogeneous array of polarizable meta-atoms in the  $z = 0$  plane, which acts as a two-dimensional electromagnetic discontinuity on the incident field created by external sources (see Fig. 2). Throughout the paper, we assume a time-harmonic dependence of the form  $e^{j\omega t}$ , where  $j^2 = -1$  is the imaginary unit.

A metasurface, described by a set of surface susceptibility components ( $\bar{\chi}_{ee}$ ,  $\bar{\chi}_{em}$ ,  $\bar{\chi}_{me}$ ,  $\bar{\chi}_{mm}$ ), can generate output fields with the desired transverse spatial dependency of  $\psi_{\text{ref/tran}}^{\text{TE/TM}}(x,y)$  in transmission/reflection mode when arbitrary input fields having the spatial dependence  $\psi_{\text{inc}}^{\text{TE/TM}}(x,y)$  excite it. In fact,  $\psi_{\text{inc}}^{\text{TE/TM}}(x,y)$  and  $\psi_{\text{ref/tran}}^{\text{TE/TM}}(x,y)$  can be considered as the input and output signals of our linear system, where the angular electromagnetic (EM) response of the metasurface processor determines the corresponding TF,  $O(k_x, k_y)$ , in the spatial Fourier domain. Actually, the TF represents the response

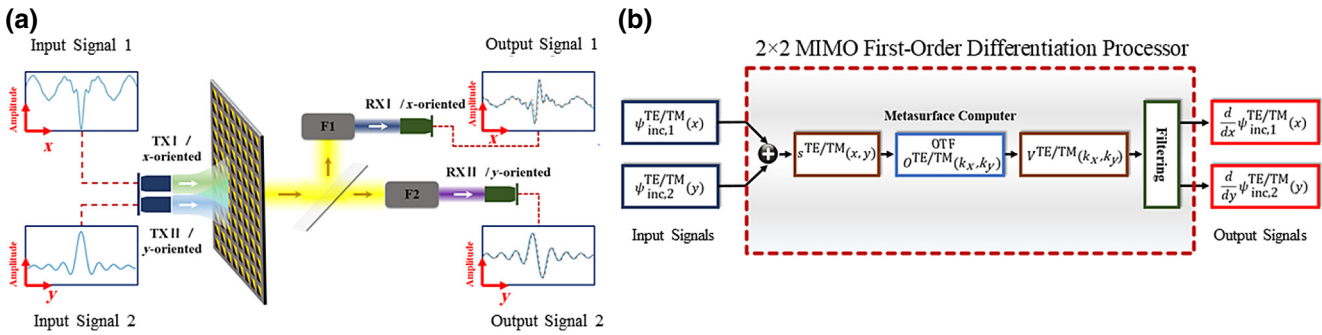


FIG. 1. (a) Schematic of the proposed spatial MIMO metasurface processor for performing real-time parallel analog signal processing. (b) The block diagram view of the  $2 \times 2$  MIMO first-order differentiation processor. Input signal 1,  $\psi_{\text{inc},1}^{\text{TE/TM}}(x)$ , and input signal 2,  $\psi_{\text{inc},2}^{\text{TE/TM}}(y)$ , have  $x$  and  $y$  variations, respectively. The input signals illuminate normally and simultaneously the metasurface processor and the transmitted waves are separated by F1 and F2, which are spatial low-pass filters related to the  $k_x$  and  $k_y$  directions, respectively. Finally,  $(d/dx)\psi_{\text{inc},1}^{\text{TE/TM}}(x)$  and  $(d/dy)\psi_{\text{inc},2}^{\text{TE/TM}}(y)$  as output signals are obtained. The processor works equally for TE or TM polarization.

to plane waves at different angles of incidence, providing a useful representation of the properties of metasurfaces [22].

Here, the solutions can be computed by  $\psi_{\text{ref/tran}}(x, y) = F^{-1} [\tilde{O}(k_x, k_y) \times F[\psi_{\text{inc}}(x, y)]]$  in which  $F$  and  $F^{-1}$  represent the operation of Fourier and inverse Fourier transform, respectively, and  $k_x$  and  $k_y$  denote the spatial frequency variables in Fourier space. Commonly, the TF provided by an array of polarizable meta-atoms has a tensorial format for both orthogonal polarizations that can be written as

$$\bar{O}^{\text{TE/TM}}(k_x, k_y) \equiv \begin{bmatrix} \tilde{u}^{\text{TE/TE}}(k_x, k_y) & \tilde{u}^{\text{TE/TM}}(k_x, k_y) \\ \tilde{u}^{\text{TM/TE}}(k_x, k_y) & \tilde{u}^{\text{TM/TM}}(k_x, k_y) \end{bmatrix}, \quad (1)$$

where  $\tilde{u}(k_x, k_y)$  refers to the functionality of the reflection ( $R$ ) or transmission ( $T$ ) coefficient of the metasurface processor from the incident wave angle. The first and second superscripts also represent the polarization of the input and output waves, respectively. The spatial TF belonging to the metasurface processor can be extracted using the GSTC formalism in which the metasurface transition conditions read [32,53–56]

$$\hat{z} \times \Delta \mathbf{H} = j\omega \mathbf{P}_{\parallel} - \hat{z} \times \nabla_{\parallel} \mathbf{M}_z, \quad (2)$$

$$\Delta \mathbf{E} \times \hat{z} = j\omega \mu \mathbf{M}_{\parallel} - \nabla_{\parallel} \left( \frac{\mathbf{P}_z}{\epsilon_0} \right) \times \hat{z}, \quad (3)$$

in which  $\Delta \mathbf{E}$  and  $\Delta \mathbf{H}$  are the difference of the electric and magnetic fields on both sides of the metasurface, respectively.  $\mathbf{P}$  and  $\mathbf{M}$  represent the electric and magnetic polarization densities induced on the metasurface. The susceptibility tensor components relate the polarization densities to

the average electric and magnetic fields on both sides of the metasurface processor as  $\mathbf{P} = \epsilon_0 \bar{\chi}_{ee} \mathbf{E}_{\text{av}} + \bar{\chi}_{em} \sqrt{\mu_0 \epsilon_0} \mathbf{H}_{\text{av}}$  and  $\mathbf{M} = \bar{\chi}_{mm} \mathbf{H}_{\text{av}} + \bar{\chi}_{me} \sqrt{\epsilon_0 / \mu_0} \mathbf{E}_{\text{av}}$ . Here,  $\epsilon_0$  and  $\eta_0$  are the permittivity and the characteristic impedance of free space, respectively. In the most general case, each susceptibility tensor appearing in Eqs. (2) and (3) includes both longitudinal and tangential components, i.e. 36 susceptibilities.

As we see in Eqs. (2) and (3) if we consider a homogeneous metasurface without normal polarization ( $P_z = M_z = 0$ ), only purely tangential polarizations exist, and no asymmetric function with respect to  $x$  coordinate ( $k_x$  for example) is allowed. In fact, in this circumstance, the synthesized TF has an even response ( $k_x^2$  for example) with respect to  $x$  coordinate. However, when we involve the  $P_z$  and  $M_z$  terms, according to Eqs. (2) and (3), the  $\partial_x = jk_x$  (or  $\partial_y = jk_y$ ) operators in  $\nabla_{\parallel}(\cdot)$  make possible a spatial asymmetric TF. To delve more deeply and have a better awareness of how the angular scattering response of a metasurface depends on its normal susceptibilities, we begin the study with a simplified but pertinent scenario. We synthesize the metasurface processor with an expected performance described by a TF specified on  $(k_x, 0)$  and  $(0, k_y)$ . For brevity and avoiding the complexity of relations, we write the relations, reflection and transmission of the metasurface, only for  $(k_x, 0)$ . Naturally, a similar procedure can be mimicked for  $(0, k_y)$ . Without loss of generality, we focus on TM-polarized illumination. The general analytical method to compute the co- and cross-polarized reflection and transmission coefficients is reported in Appendix A. As can be noticed from Eqs. (A1)–(A7), the physical and insightful understanding of these equations is sophisticated due to complexity of involving full tensor susceptibility components. Therefore, we only consider the susceptibility components that

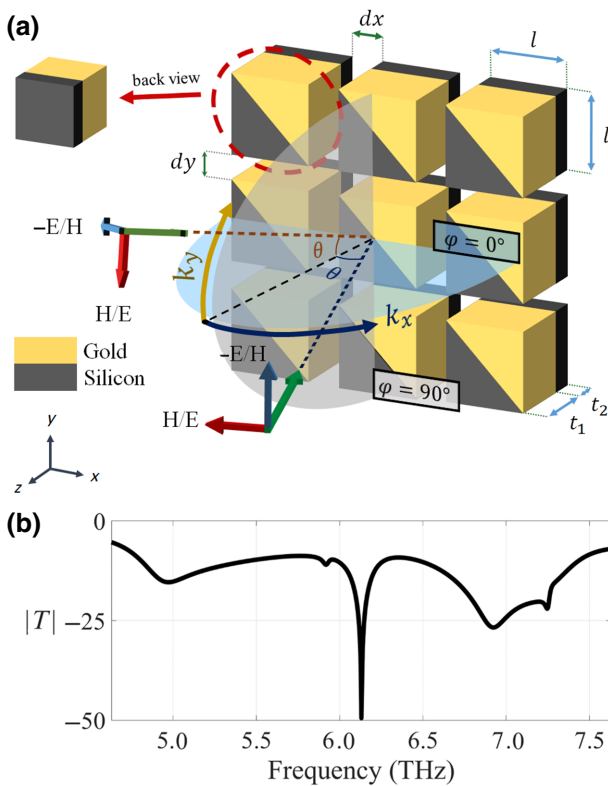


FIG. 2. (a) Realization of the MIMO metasurface processor at a wavelength  $\lambda_0 = 48.935 \mu\text{m}$ . The schematic shows an array of designed meta-atoms in the  $x$ - $y$  plane. The metasurface is excited by TM- or TE-polarized electromagnetic waves. The geometric parameters are  $dx = dy = 4 \mu\text{m}$ ,  $l = 15 \mu\text{m}$ ,  $t_1 = 11 \mu\text{m}$ , and  $t_2 = 4 \mu\text{m}$ . The period of meta-atom ( $= 0.38\lambda_0$ ) satisfies the homogenization condition related to meta-atom period [51,52]. (b) The magnitude of the transmission versus frequency for both orthogonal polarizations around  $k_x$  and  $k_y$ .

preserve the polarization of illuminated wave for better physical and insightful understanding:

$$\bar{\chi}_{ee} = \begin{pmatrix} \chi_{ee}^{xx} & 0 & \chi_{ee}^{xz} \\ 0 & 0 & 0 \\ \chi_{ee}^{zx} & 0 & \chi_{ee}^{zz} \end{pmatrix}, \quad \bar{\chi}_{em} = \begin{pmatrix} 0 & \chi_{em}^{xy} & 0 \\ 0 & 0 & 0 \\ 0 & \chi_{em}^{zy} & 0 \end{pmatrix}, \quad (4)$$

$$\bar{\chi}_{me} = \begin{pmatrix} 0 & 0 & 0 \\ \chi_{me}^{yx} & 0 & \chi_{me}^{yz} \\ 0 & 0 & 0 \end{pmatrix}, \quad \bar{\chi}_{mm} = \begin{pmatrix} 0 & 0 & 0 \\ 0 & \chi_{mm}^{yy} & 0 \\ 0 & 0 & 0 \end{pmatrix}.$$

The reciprocity conditions enforce  $\bar{\chi}_{ee}^T = \bar{\chi}_{ee}$ ,  $\bar{\chi}_{mm}^T = \bar{\chi}_{mm}$ . In this case, the reflection and transmission coefficients can be expressed in terms of the metasurface susceptibilities as shown in Ref. [32], and are given by

$$\gamma = 2[k_z^2 \chi_{ee}^{xx} + k_z^2 \chi_{ee}^{zz} + k_0^2 \chi_{mm}^{yy}] + k_0^2 (\chi_{ee}^{xx} \chi_{mm}^{yy} + \chi_{me}^{xy})^2 - j k_z [k_z^2 (\chi_{ee}^{xz^2} - \chi_{ee}^{xx} \chi_{ee}^{zz}) + 4], \quad (5)$$

$$\mathbf{T}(k_x, 0) = \frac{j k_z}{\gamma} \{k_z^2 (\chi_{ee}^{xz^2} - \chi_{ee}^{xx} \chi_{ee}^{zz}) + (2j - k_0 \chi_{em}^{xy})(2j + k_0 \chi_{em}^{xy}) + k_x [\chi_{ee}^{xz} (2j - k_0 \chi_{em}^{xy}) + \chi_{ee}^{xz} (2j + k_0 \chi_{em}^{xy})] - k_0^2 \chi_{ee}^{yy} \chi_{mm}^{xx}\}, \quad (6)$$

$$\mathbf{R}(k_x, 0) = \frac{2}{\gamma} \{k_z^2 \chi_{ee}^{zz} - k_z^2 \chi_{ee}^{xx} + 2k_z k_0 \chi_{em}^{xy} + k_0^2 \chi_{mm}^{yy}\}. \quad (7)$$

As can be noticed from Eqs. (5) and (6), the presence of nonzero  $\chi_{ee}^{xz}$  component makes the transmission transfer function odd with respect to the  $k_x$  variable, creating an asymmetric function of  $\theta$ . The other normal susceptibility components cannot be used to break the angular symmetry of the transmission transfer function, e.g.  $\chi_{ee}^{zz}$  induces a term proportional to  $k_z^2$  in the relations, which implies an even-symmetric function of  $\theta$ . We conclude that the normal polarizability component  $\chi_{ee}^{xz}$  is mandatory for breaking the angular symmetry of the transmission of the metasurface.

From a realization point of view, there are fruitful relationships between the structural symmetries of the metasurface scattering meta-atoms and the corresponding symmetries of their angular scattering response. Geometrically, three types of symmetries are conceivable for the constituent meta-atoms: a reflection symmetry through the  $z$  axis ( $\sigma_z$ ), a  $180^\circ$  rotation symmetry around the  $y$  axis ( $C_2$ ), and a reflection symmetry through the  $x$  axis ( $\sigma_x$ ) [32]. Regarding a reciprocal metasurface, the angular spectrum of the reflection coefficient exposes a  $\sigma_z$  symmetry, while that of the transmission coefficient has a  $C_2$  symmetry. Most importantly, a metasurface with both normal and tangential susceptibilities is macroscopically achieved when the occupying meta-atoms do not microscopically render any geometric symmetry.

In fact, when the meta-atoms are deprived of the mentioned geometric symmetry the resultant metasurface will present  $\chi_{ee}^{xz}$  (or  $\chi_{ee}^{zx}$ ). Breaking both vertical and horizontal mirror symmetries of meta-atoms is therefore required for realizing the asymmetric TF response [32]. Along this line of thought, we design an asymmetric meta-atom [Fig. 2(b)] comprised of two materials [gold [57] and silicon ( $\epsilon_r = 12$ )], for operation at  $\lambda_0 = 48.935 \mu\text{m}$ . The presented meta-atom would be neither  $\sigma_z$  symmetric nor  $C_2$  symmetric. In fact, we break both vertical and horizontal mirror symmetries to enable a nonzero normal polarization,  $\chi_{ee}^{xz}$ , reaching an asymmetric TF.

Another important point about the structural symmetry of the designed meta-atom is that the meta-atom is symmetric with respect to the  $x = y$  line. This symmetric feature is of importance for realizing parallel analog signal computing. This point can be figured out from Fig. 3, which shows the amplitude and phase of electric field profiles at plane  $z = 0$  for both  $\theta = 10^\circ$  and  $-10^\circ$ . By comparing Figs. 3(a) and 3(b) with Figs. 3(e) and 3(f), the

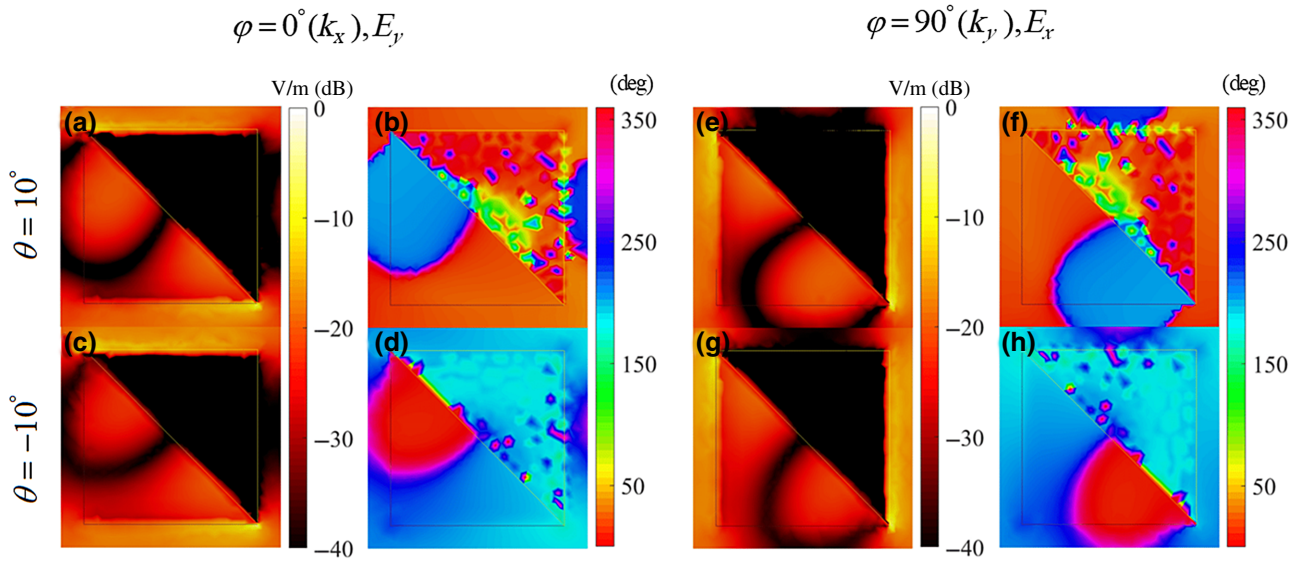


FIG. 3. Electric field profiles (V/m in dB scale) at plane  $z = 0$  (top surface of meta-atoms) when  $\theta = 10^\circ$  and  $-10^\circ$ . (a),(c),(e),(g) Amplitude of electric fields for  $\theta = 10^\circ$  and  $-10^\circ$ . (b),(d),(f),(h) Phase information (degrees) of electric fields.

symmetric feature with respect to the  $x = y$  line is obvious. In fact, as we expected, the mirror image of Figs. 3(a) and 3(b) can be seen in Figs. 3(e) and 3(f). A similar discussion for Figs. 3(c) and 3(d) and Figs. 3(g) and 3(h) is valid. In summary, due to this geometric symmetry, we expect effectively to attain the same transmission response in  $x$  and  $y$  directions, which enables parallel analog signal processing.

In the following, we demonstrate some possible wave-based functionalities that can be unlocked by the proposed metasurface processor, as the fundamental block realizing

the operator of choice. One of the most important mathematical functions that has been less explored in the literature is the first-order differentiation operator whose spatial TF can be written as  $O(k_x, 0) = \alpha j k_x$  and  $O(0, k_y) = \beta j k_y$ , where  $\alpha$  and  $\beta$  are complex constant coefficients that represent the gain values of the first-order differentiation operators.

Figure 4 displays the synthesized and required TFs for transmitting the first-order derivation of the input field profile for both TE and TM polarizations. The structural specifications of the meta-atom lead to resonance for

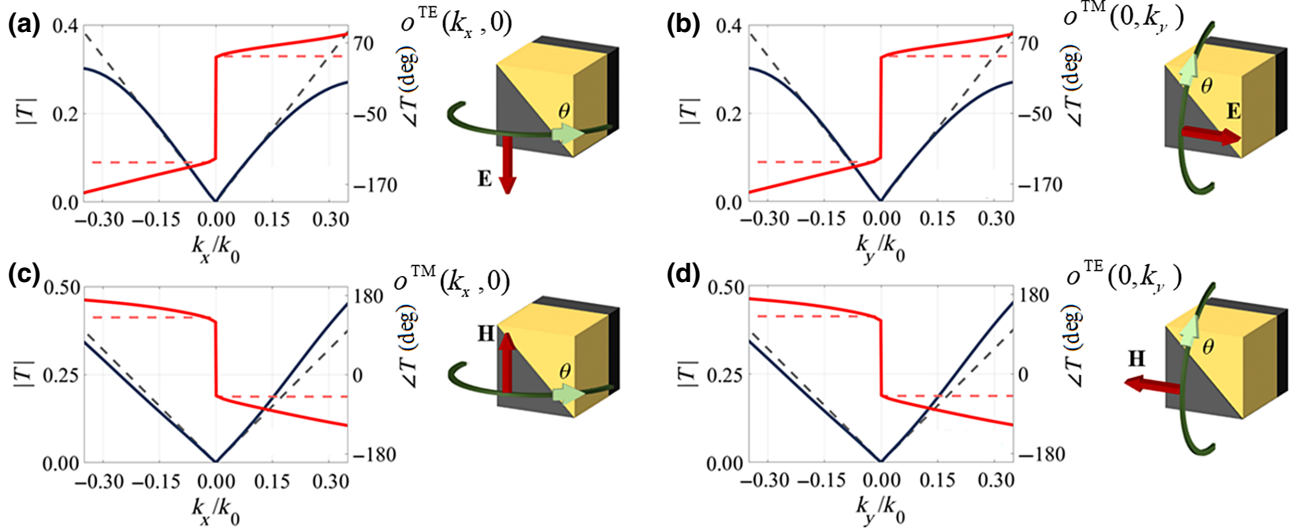


FIG. 4. Synthesized TF. (a),(c) The amplitude (black) and phase (red) of the synthesized TF( $k_x, 0$ ) associated with the first-order differentiation realized by the metasurface processor for TE and TM polarization, respectively. (b),(d) Similar plots for TF( $0, k_y$ ). The synthesized and ideal TFs are indicated with solid and dashed lines, respectively.

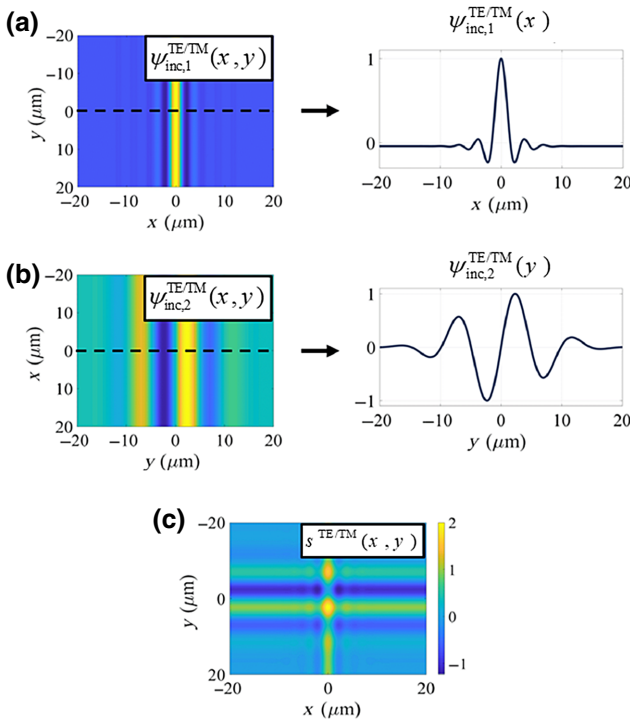


FIG. 5. Input signals. The (a) first and (b) second arbitrary incident field profiles. (c) Combination of both input signals in the  $x$ - $y$  plane for both orthogonal polarization states.

normal incident waves ( $k_x = k_0$ ). As we can see in Fig. 4, the amplitude of the transmission coefficient is infinitesimal at the normal incident angle and it linearly increases when the incident angle changes. The  $180^\circ$  phase difference between  $k_t > 0$  and  $k_t < 0$  of the TF indicates asymmetric, odd, angular response of the TF. Based on the right-hand sides of Eqs. (2) and (3), this asymmetric transmission response of the metasurface with respect to  $k_x$  or  $k_y$  shows strong values of normal susceptibility components in the physical meta-atom depicted in Fig. 2. In addition, the tangential susceptibility components are extracted and shown in Appendix B. The results are simulated using CST full-wave commercial software.

Here, as we discussed above, the geometry of the proposed meta-atom enables us to have the same synthesized TF for  $y$  directions, which is important for our goal (see Fig. 4). The proposed meta-atom can elaborately mimic the required  $k_x$  and  $k_y$  dependency of first-order differentiator (see Fig. 4). The phase and amplitude of the resulting transmission coefficient are plotted for both orthogonal polarizations in Figs. 4(a)–4(d). An excellent agreement between the synthesized TF and the exact TF is achieved as long as the normalized spectral beamwidth of the input signals lies within  $|W/k_0| < 0.35$ . As we can see in Fig. 4, the values of  $\alpha$  and  $\beta$  are  $|\alpha| \approx |\beta| \approx 1$ .

Also, this is clear from the point of view of the electric field profile, which is plotted in Fig. 3; by comparing Figs.

3(a) and 3(b) with Figs. 3(c) and 3(d), as expected, we see the same amplitude and  $180^\circ$  phase difference between  $\theta = 10^\circ$  and  $\theta = -10^\circ$ . The same discussion for Figs. 3(e) and 3(f) and Figs. 3(g) and 3(h) for  $\phi = 90$  is valid.

### III. REAL-TIME PARALLEL ANALOG SIGNAL PROCESSING

In this section, we explore a  $2 \times 2$  MIMO first-order differentiation processor, which enables independent parallel channels for signal processing, a key result of this paper.

Our final goal is performing the first-order differentiation simultaneously on two distinct input signals,  $\psi_{\text{inc},1}^{\text{TE/TM}}(x)$  and  $\psi_{\text{inc},2}^{\text{TE/TM}}(y)$ , regardless of the polarization chosen (TE/TM means that we have the freedom to choose either TE or TM polarization). In fact, we start from a combination of two arbitrary input signals [ $s^{\text{TE/TM}}(x,y) = \psi_{\text{inc},1}^{\text{TE/TM}}(x) + \psi_{\text{inc},2}^{\text{TE/TM}}(y)$ ] created by two sources, one of which has an  $x$  variation [ $\psi_{\text{inc},1}^{\text{TE/TM}}(x)$ ] and the other a  $y$  variation [ $\psi_{\text{inc},2}^{\text{TE/TM}}(y)$ ]. Therefore, by using a Fourier transform, we can theoretically write

$$S^{\text{TE/TM}}(k_x, k_y) = \Psi_{\text{inc},1}^{\text{TE/TM}}(k_x) \delta(k_y) + \Psi_{\text{inc},2}^{\text{TE/TM}}(k_y) \delta(k_x), \quad (8)$$

where  $S^{\text{TE/TM}}(k_x, k_y)$  is the combination of two input signals in Fourier domain and  $\delta(\cdot)$  is the Dirac  $\delta$  function. Based on the synthesized TF (see Fig. 4), the two-dimensional  $O^{\text{TE/TM}}(k_x, k_y)$  can be written as follows:

$$O^{\text{TE/TM}}(k_x, k_y) = \begin{cases} \alpha j k_x & k_y = 0 \\ \beta j k_y & k_x = 0 \\ W(k_x, k_y) & k_x, k_y \neq 0, \end{cases} \quad (9)$$

where  $W(k_x, k_y)$  corresponds to the synthesized TF at  $(k_x, k_y \neq 0)$ . The theoretical method for susceptibilities extraction for first-order differentiation operation is presented in Appendix C. As we mentioned before, due to the fact that our input signals only have  $x$  or  $y$  variations, the synthesized TF associated with the metasurface processor needs to have the first-order differentiator function only in  $(k_x, 0)$  and  $(0, k_y)$ . Therefore, the expression for  $W(k_x, k_y)$  is unimportant for our purpose. By multiplying the TF by  $S^{\text{TE/TM}}(k_x, k_y)$ , the output  $V(k_x, k_y)$  can be written as follows:

$$V(k_x, k_y) = O^{\text{TE/TM}}(k_x, k_y) S^{\text{TE/TM}}(k_x, k_y) = \begin{cases} \alpha j k_x \Psi_{\text{inc},1}^{\text{TE/TM}}(k_x) \delta(k_y) + \alpha j k_x \Psi_{\text{inc},2}^{\text{TE/TM}}(k_y) \delta(k_x) & k_y = 0 \\ \beta j k_y \Psi_{\text{inc},1}^{\text{TE/TM}}(k_x) \delta(k_y) + \beta j k_y \Psi_{\text{inc},2}^{\text{TE/TM}}(k_y) \delta(k_x) & k_x = 0 \\ 0 & k_x, k_y \neq 0. \end{cases} \quad (10)$$

Based on the definition of the Dirac  $\delta$  function [58] and after some mathematical manipulations we have  $V(k_x, k_y) = \alpha j k_x \Psi_{\text{inc},1}^{\text{TE/TM}}(k_x) \delta(k_y) + \beta j k_y \Psi_{\text{inc},2}^{\text{TE/TM}}(k_y) \delta(k_x)$ ; therefore, by using inverse Fourier transform,  $v(x, y)$  can be written as follows [10,17]:

$$v(x, y) = \int_{-\infty}^{+\infty} \int_{-\infty}^{+\infty} \alpha j k_x \Psi_{\text{inc},1}^{\text{TE/TM}}(k_x) \delta(k_y) e^{-j k_x x} e^{-j k_y y} dk_x dk_y + \int_{-\infty}^{+\infty} \int_{-\infty}^{+\infty} \beta j k_y \Psi_{\text{inc},2}^{\text{TE/TM}}(k_y) \delta(k_x) e^{-j k_x x} e^{-j k_y y} dk_x dk_y \quad (11)$$

$$= \alpha \frac{d}{dx} \psi_{\text{inc},1}^{\text{TE/TM}}(x) + \beta \frac{d}{dy} \psi_{\text{inc},2}^{\text{TE/TM}}(y). \quad (12)$$

Finally, by using two SLPFs, we can extract and separate our desired output signals as follows:

$$k_y\text{-SPLF}\{v(x, y)\} = \alpha \frac{d}{dx} \psi_{\text{inc},1}^{\text{TE/TM}}(x), \quad (13)$$

$$k_x\text{-SPLF}\{v(x, y)\} = \beta \frac{d}{dy} \psi_{\text{inc},2}^{\text{TE/TM}}(y). \quad (14)$$

Conceptually, a schematic of the  $2 \times 2$  MIMO first-order differentiation processor is shown in Fig. 1(b). Consider a computational and realistic scenario in which two different input signals in  $x$  and  $y$  directions [ $\psi_{\text{inc},1}^{\text{TE/TM}}(x)$  and  $\psi_{\text{inc},2}^{\text{TE/TM}}(y)$ ] collide to a reciprocal metasurface from the normal direction. Upon interacting with the metasurface processor and depending on the  $k_t$  modulation of the spatial TF dictated by an array of asymmetric metatoms, the combination of input signals [ $s^{\text{TE/TM}}(x, y)$ ] is mapped along  $k_x$  and  $k_y$  directions of the output signal [ $V^{\text{TE/TM}}(k_x, k_y)$ ] in Fourier domain [see Eq. (10)]. Thereafter, desired output signals [ $(d/dx)\psi_{\text{inc},1}^{\text{TE/TM}}(x)$  and

$(d/dy)\psi_{\text{inc},2}^{\text{TE/TM}}(y)$ ] can be obtained and separated after passing from SLPFs.

To demonstrate the real-time parallel computing capability of the proposed scheme, we consider as inputs the two arbitrary signals shown in Figs. 5(a) and 5(b). Simultaneously emitted by two sources, they combine into the two-dimensional function shown in Fig. 5(c). This field illuminates the metasurface processor, which generates the output image,  $v^{\text{TE/TM}}(x, y)$  [see Figs. 6(a) and 7(a)]. Consistent with our design, the  $V^{\text{TE/TM}}(k_x, k_y)$  image only has values along  $k_x$  and  $k_y$  directions [see Figs. 6(b) and 7(b) and Eq. (10)]. Subsequently, by using the SLPFs along  $k_x$  and  $k_y$ , the final output signals are generated, as shown in Figs. 6 and 7 for TE and TM polarizations, respectively. One should note that many prior works have introduced designs for appropriate SLPFs based on a simple single metasurface [11,59,60]. The extraction performance of desired output signals depends on these SLPFs. Actually, the sharper the SLPFs, the better the extraction and separation performance. For this reason, we cascade two first-order integrator metasurfaces based on Ref. [60]

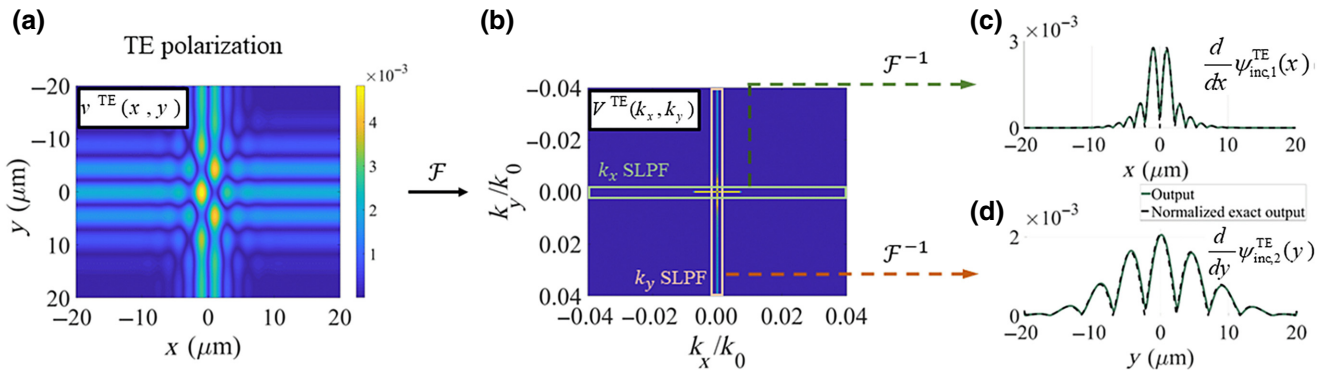


FIG. 6. Output signals. The TE-polarized transmitted image in space domain (a) and in Fourier domain (b). Extracted output signals after passing from (c)  $k_x$ -SLPF and (d)  $k_y$ -SLPF.

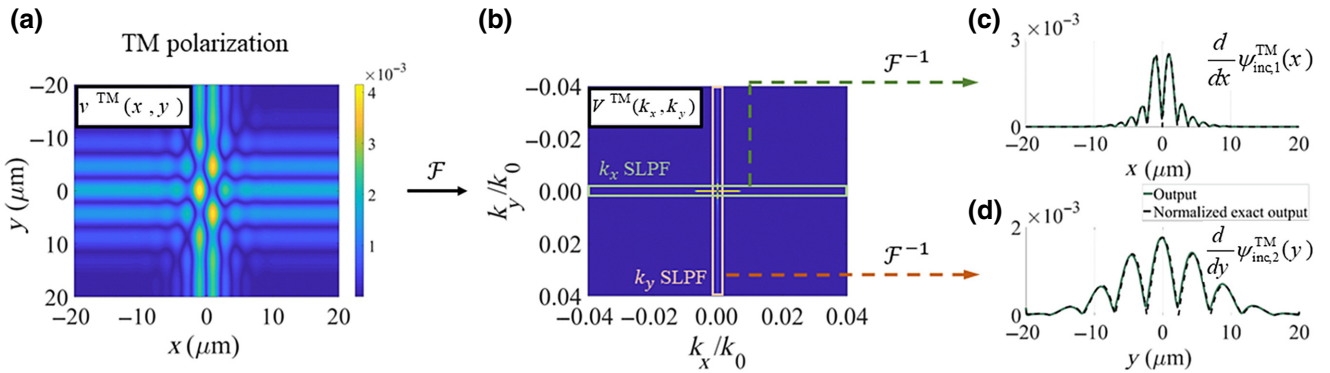


FIG. 7. Output signals. The TM-polarized transmitted image in space domain (a) and in Fourier domain (b). Extracted output signals after passing from (c)  $k_x$ -SLPF and (d)  $k_y$ -SLPF.

to realize sharp SLPFs. The transmission coefficients of desired multilayer dielectric SLPFs are shown in Fig. 8. In addition, the transmission coefficients and output signals for a graphene-based SLPF are shown in Appendix D. It is clear that due to using the low-thickness graphene-based SLPF, the final size of the  $2 \times 2$  MIMO system is still low profile (smaller than the operation wavelength). For the sake of comparison, Figs. 6(c) and 6(d) and Figs. 7(c) and 7(d) also plot the exact and the output signals for both orthogonal polarizations. An excellent agreement between simulated and benchmark results has been achieved when the normalized spectral beamwidth of the input signals lies within  $|W| < 0.35k_0$ .

#### IV. CONCLUSION

In summary, a  $2 \times 2$  MIMO first-order differentiation processor is elaborately designed to be utilized in a spatial analog computing platform for realizing massively parallel processing. Through synthesizing proper asymmetric

meta-atom, based on GSTC and susceptibility tensors, the metasurface processor is able to realize the required phases and amplitudes of the TF associated with the first-order differentiation operation. This analog MIMO metasurface processor with asymmetric response can perform spatial differentiation on two distinct input signals (in  $x$  and  $y$  directions) at the same time for both orthogonal polarization states. The proposed theoretical framework foretastes that the presented design overcomes the substantial restrictions imposed by previous investigations, such as large architectures arising from the need for additional sub-blocks, slow responses, and, most importantly, supporting only one/single input and a certain incident polarization. The numerical results prove that the proposed metasurface processor may be thought of as an efficient and flexible host for use in the field of real-time parallel optical signal processing.

#### APPENDIX A: GENERAL AND ANALYTICAL METHOD TO COMPUTE THE TRANSMISSION AND REFLECTION COEFFICIENTS

To exploit the complete potential of the metasurface boundary, each susceptibility tensor of Eqs. (2) and (3) includes both normal and tangential components, i.e. 36 scalar susceptibilities that can be written as

$$\bar{\chi}_{ee} = \begin{bmatrix} \chi_{ee}^{xx} & \chi_{ee}^{xy} & \chi_{ee}^{xz} \\ \chi_{ee}^{yx} & \chi_{ee}^{yy} & \chi_{ee}^{yz} \\ \chi_{ee}^{zx} & \chi_{ee}^{zy} & \chi_{ee}^{zz} \end{bmatrix}, \quad \bar{\chi}_{em} = \begin{bmatrix} \chi_{em}^{xx} & \chi_{em}^{xy} & \chi_{em}^{xz} \\ \chi_{em}^{yx} & \chi_{em}^{yy} & \chi_{em}^{yz} \\ \chi_{em}^{zx} & \chi_{em}^{zy} & \chi_{em}^{zz} \end{bmatrix}, \quad (A1)$$

$$\bar{\chi}_{me} = \begin{bmatrix} \chi_{me}^{xx} & \chi_{me}^{xy} & \chi_{me}^{xz} \\ \chi_{me}^{yx} & \chi_{me}^{yy} & \chi_{me}^{yz} \\ \chi_{me}^{zx} & \chi_{me}^{zy} & \chi_{me}^{zz} \end{bmatrix}, \quad \bar{\chi}_{mm} = \begin{bmatrix} \chi_{mm}^{xx} & \chi_{mm}^{xy} & \chi_{mm}^{xz} \\ \chi_{mm}^{yx} & \chi_{mm}^{yy} & \chi_{mm}^{yz} \\ \chi_{mm}^{zx} & \chi_{mm}^{zy} & \chi_{mm}^{zz} \end{bmatrix}. \quad (A2)$$

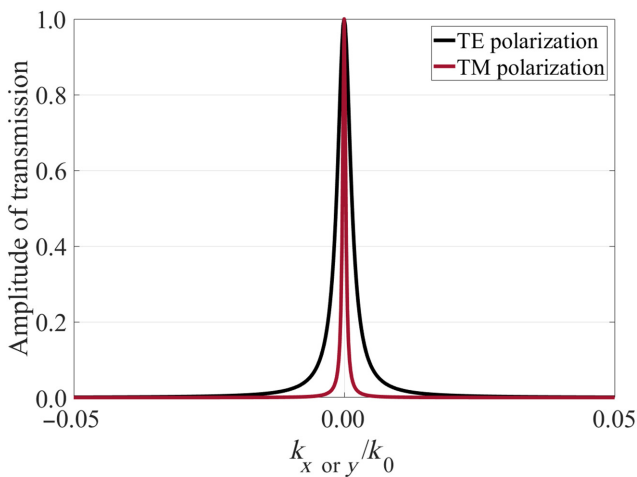


FIG. 8. Transmission coefficients of  $k_x$ -SLPF and  $k_y$ -SLPF for both TE and TM states.

After some algebraic manipulations, the reflection coefficient of the bianisotropic metasurface can be represented

by a spatially dispersive function of the scalar susceptibilities. The blue- and red-marked susceptibilities manifest themselves in the reflection coefficient of the metasurface upon illumination by TE- and TM-polarized incidences, respectively. By assuming a general bianisotropic metasurface exciting both orthogonal polarizations and after some algebraic manipulations, we can combine Eqs. (2) and (3) to compute reflection and transmission coefficients based

on all involved susceptibilities:

$$\begin{bmatrix} -\Delta H_y \\ \Delta H_x \\ \Delta E_y \\ -\Delta E_x \end{bmatrix} = T \begin{bmatrix} E_{x,\text{av}} \\ E_{y,\text{av}} \\ E_{z,\text{av}} \\ H_{x,\text{av}} \\ H_{y,\text{av}} \\ H_{z,\text{av}} \end{bmatrix}, \quad (\text{A3})$$

$$T = \begin{bmatrix} j\omega\varepsilon_0\chi_{ee}^{xx} & j\omega\varepsilon_0\chi_{ee}^{xy} & j\omega\varepsilon_0\chi_{ee}^{xz} & jk_0\chi_{em}^{xx} & jk_0\chi_{em}^{xy} & jk_0\chi_{em}^{xz} \\ j(\omega\varepsilon_0\chi_{me}^{yx} + k_x\chi_{me}^{zx}/\eta_0) & j(\omega\varepsilon_0\chi_{me}^{yy} + k_x\chi_{me}^{zy}/\eta_0) & j(\omega\varepsilon_0\chi_{me}^{yz} + k_x\chi_{me}^{zz}/\eta_0) & j(\omega\varepsilon_0\chi_{mm}^{yx} + k_x\chi_{mm}^{zx}) & j(\omega\varepsilon_0\chi_{mm}^{yy} + k_x\chi_{mm}^{zy}) & j(\omega\varepsilon_0\chi_{mm}^{yz} + k_x\chi_{mm}^{zz}) \\ jk_0\chi_{me}^{xx} & jk_0\chi_{me}^{xy} & jk_0\chi_{me}^{xz} & j\omega\mu_0\chi_{mm}^{xx} & j\omega\mu_0\chi_{mm}^{xy} & j\omega\mu_0\chi_{mm}^{xz} \\ j(k_0\chi_{me}^{yx} - k_x\chi_{ee}^{zx}) & j(k_0\chi_{me}^{yy} - k_x\chi_{ee}^{zy}) & j(k_0\chi_{me}^{yz} - k_x\chi_{ee}^{zz}) & j(\omega\mu_0\chi_{mm}^{yx} - \eta_0k_x\chi_{em}^{zx}) & j(\omega\mu_0\chi_{mm}^{yy} - \eta_0k_x\chi_{em}^{zy}) & j(\omega\mu_0\chi_{mm}^{yz} - \eta_0k_x\chi_{em}^{zz}) \end{bmatrix}. \quad (\text{A4})$$

Within the spatial Fourier domain, the angular-dependent co- and cross-polarized reflection and transmission coefficients can be expressed as

$$\begin{bmatrix} R^{\text{TM}\rightarrow\text{TM}}(k_x, 0) \\ R^{\text{TM}\rightarrow\text{TE}}(k_x, 0) \\ T^{\text{TM}\rightarrow\text{TM}}(k_x, 0) \\ T^{\text{TM}\rightarrow\text{TE}}(k_x, 0) \end{bmatrix} = \left[ \psi_1 - T\psi_2 \right]^{-1} \times \left[ C_1 + TC_2 \right], \quad (\text{A5})$$

in which

$$\psi_1 = \begin{bmatrix} 1/\eta & 0 & -1/\eta & 0 \\ 0 & \cos(\theta)/\eta & 0 & \cos(\theta)/\eta \\ 0 & 1 & 0 & 1 \\ -\cos(\theta) & 0 & -\cos(\theta) & 0 \end{bmatrix}, \quad C_1 = \begin{bmatrix} -1/\eta \\ 0 \\ 0 \\ \cos(\theta) \end{bmatrix}, \quad (\text{A6})$$

$$\psi_2 = \begin{bmatrix} -\cos(\theta)/2 & 0 & \cos(\theta)/2 & 0 \\ 0 & -1/2 & 0 & -1/2 \\ -\sin(\theta)/2 & 0 & -\sin(\theta)/2 & 0 \\ 0 & -\cos(\theta)/(2\eta) & 0 & \cos(\theta)/(2\eta) \\ 1/(2\eta) & 0 & 1/(2\eta) & 0 \\ 0 & -\sin(\theta)/(2\eta) & 0 & -\sin(\theta)/(2\eta) \end{bmatrix},$$

$$C_2 = \begin{bmatrix} \cos(\theta)/2 \\ 0 \\ -\sin(\theta)/2 \\ 0 \\ 1/(2\eta) \\ 0 \end{bmatrix}. \quad (\text{A7})$$

## APPENDIX B: SUSCEPTIBILITY COMPONENTS OF THE PROPOSED META-ATOM

The tangential susceptibility components of the proposed meta-atom are extracted and shown in Fig. 9.

## APPENDIX C: SUSCEPTIBILITY EXTRACTION FOR FIRST-ORDER DIFFERENTIATION OPERATION

Firstly, consider a uniform mono-anisotropic, diagonal, and hence nongyrotropic and reciprocal metasurface with

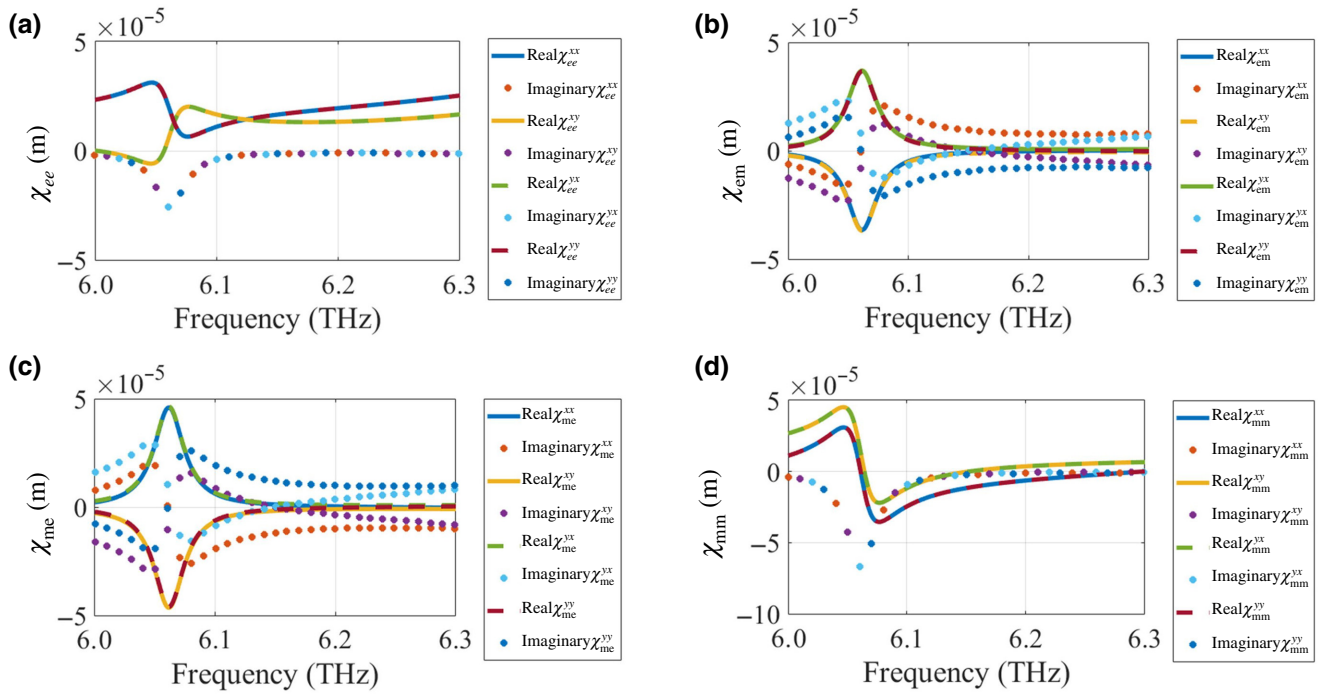


FIG. 9. Extracted tangential susceptibility components of the proposed meta-atom. Electric (a), electromagnetic (b), magnetoelectric (c), and magnetic (d) susceptibility components.

six scalar independent susceptibility components:

$$\bar{\bar{\chi}}_{ee} = \begin{pmatrix} \chi_{ee}^{xx} & 0 & 0 \\ 0 & \chi_{ee}^{yy} & 0 \\ 0 & 0 & \chi_{ee}^{zz} \end{pmatrix}, \quad (C1)$$

$$\bar{\bar{\chi}}_{mm} = \begin{pmatrix} \chi_{mm}^{xx} & 0 & 0 \\ 0 & \chi_{mm}^{yy} & 0 \\ 0 & 0 & \chi_{mm}^{zz} \end{pmatrix}. \quad (C2)$$

For such a simple metasurface, the nonlocal co-polarized scattering coefficients of Eqs. (2) and (3) can be re-expressed in an explicit form [13]:

$$\tilde{T}^{\text{TM/TM}}(k_x, 0) = \frac{k_z(4 + \chi_{ee}^{xx}\chi_{mm}^{yy}k_0^2 + \chi_{ee}^{xx}\chi_{ee}^{zz}k_x^2)}{(2j - \chi_{ee}^{xx}k_z)(\chi_{mm}^{yy}k_0^2 + \chi_{ee}^{zz}k_x^2 - 2jk_z)}, \quad (C3)$$

$$\tilde{T}^{\text{TE/TE}}(k_x, 0) = \frac{k_z(4 + \chi_{mm}^{xx}\chi_{ee}^{yy}k_0^2 + \chi_{mm}^{xx}\chi_{mm}^{zz}k_x^2)}{(2j - \chi_{mm}^{xx}k_z)(\chi_{ee}^{yy}k_0^2 + \chi_{mm}^{zz}k_x^2 - 2jk_z)}, \quad (C4)$$

$$\tilde{R}^{\text{TM/TM}}(k_x, 0) = \frac{2j(\chi_{mm}^{yy}k_0^2 + \chi_{ee}^{zz}k_x^2 - \chi_{ee}^{xx}k_z^2)}{(2j - \chi_{ee}^{xx}k_z)(\chi_{mm}^{yy}k_0^2 + \chi_{ee}^{zz}k_x^2 - 2jk_z)}, \quad (C5)$$

$$\tilde{R}^{\text{TE/TE}}(k_x, 0) = \frac{2j(\chi_{ee}^{yy}k_0^2 + \chi_{mm}^{zz}k_x^2 - \chi_{mm}^{xx}k_z^2)}{(2j - \chi_{mm}^{xx}k_z)(\chi_{ee}^{yy}k_0^2 + \chi_{mm}^{zz}k_x^2 - 2jk_z)}. \quad (C6)$$

Assuming  $|k_x| \ll k_0$  and using the Taylor expansion of the co-polarized transmission coefficient of the employed metasurface around  $k_x = 0$ , we have

$$\tilde{T}^{\text{TM/TM}}(k_x) \simeq \tilde{T}^{\text{TM/TM}}(0) + k_x \times \frac{d\tilde{T}^{\text{TM/TM}}}{dk_x}(0) + O(k_x^2). \quad (C7)$$

By eliminating the first term of (C7), we have

$$\tilde{T}^{\text{TM/TM}}(0) \simeq \frac{q'(0)p(0)}{u(0)v(0)} \times k_x + O(k_x^2), \quad (C8)$$

where

$$\begin{aligned} p(k_x) &= \sqrt{k_0^2 - k_x^2}, \\ q(k_x) &= 4 + \chi_{ee}^{xx}\chi_{mm}^{yy}k_0^2 + \chi_{ee}^{xx}\chi_{ee}^{zz}k_y^2, \\ u(k_x) &= 2j - \chi_{ee}^{xx}\sqrt{k_0^2 - k_x^2}, \\ v(k_x) &= \chi_{mm}^{yy}k_0^2 + \chi_{ee}^{zz}k_x^2 - j\sqrt{k_0^2 - k_x^2}. \end{aligned} \quad (C9)$$

Therefore, the spatial dispersion of the transmission coefficient emulates the desired GF associated with the first-order differentiation, i.e.  $\tilde{G}_{\text{des}}(k_x) = j(k_x)$  around  $k_x = 0$ .

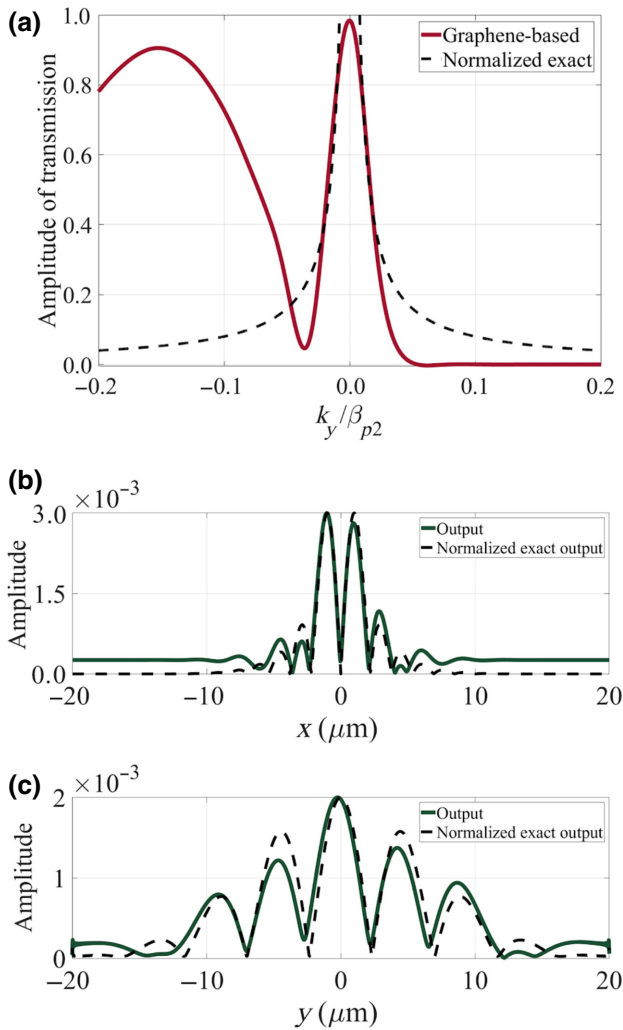


FIG. 10. (a) Transmission coefficients of graphene-based SLPF and ideal SLPF. Extracted output signals after passing from (b)  $k_x$  and (c)  $k_y$  graphene-based SLPFs.

Indeed, the angular operational region of the designed differentiator is around the zero(s) of  $q(k_x)$ , i.e. where

$$4 + \chi_{ee}^{xx} \chi_{mm}^{yy} k_0^2 = 0 \quad (\text{C10})$$

condition is satisfied. Similar conditions can be simply obtained for  $\tilde{R}^{\text{TE/TE}}(k_x, 0)$ ,  $\tilde{R}^{\text{TM/TM}}(k_x, 0)$ , and  $\tilde{T}^{\text{TE/TE}}(k_x, 0)$ . For dual-polarized operation in reflection or transmission mode, both TE and TM conditions must be met, simultaneously. Also, a similar approach can be mimicked for  $(0, k_y)$ .

In the following, a general optimization approach for susceptibility extraction is introduced. We seek for those susceptibilities for which the difference between the desired GF (here  $jk_x$ , the first-order differentiation operation) and the synthesized one, i.e. the transmission or reflection coefficient of the metasurface obtained from Eq. (A5), is minimized within a predetermined spectral range.

The error function is defined as the sum of squares of the differences at a finite number of  $N$  samples for both real and imaginary parts:

$$E = \sum_{i=1}^N w_{\text{Re}} \left\{ \text{Re} \left[ \tilde{G}_{\text{des}}(k_x) - \tilde{H}_{\text{met}}(k_x) \right] \right\}^2 + \sum_{i=1}^N w_{\text{Im}} \left\{ \text{Im} \left[ \tilde{G}_{\text{des}}(k_x) - \tilde{H}_{\text{met}}(k_x) \right] \right\}^2. \quad (\text{C11})$$

Here,  $\tilde{H}_{\text{met}}(k_x)$  refers to the spatially dispersive reflection,  $\tilde{R}_{\text{met}}(k_x)$ , or transmission,  $\tilde{T}_{\text{met}}(k_x)$ , coefficient of the bianisotropic metasurface obtained from Eq. (A5) and  $\tilde{G}_{\text{des}}(k_x)$  indicates the transfer function describing the operator(s) of choice. Also,  $w_{\text{Re}}$  and  $w_{\text{Im}}$  represent the weight coefficients that can be established to selectively find the real and imaginary parts, respectively. This optimization problem can be solved with the Nelder-Mead simplex algorithm or other gradient-based methods.

#### APPENDIX D: GRAPHENE-BASED SLPF

Similar to Ref. [60], we assume two graphene-based metasurfaces as a SLPF with typical values of  $\sigma_{g1} = 0.00033i$  and  $\sigma_{g2} = 0.00022i$  and distance  $d = 3 \mu\text{m}$  between them (for more detail, see Ref. [60]). The Green's function of the graphene-based SLPF is shown in Fig. 10. In addition, the corresponding output signals for both input signals and comparisons with exact solutions are accomplished.

As we can see in Fig. 10, there is an excellent agreement between exact and output signals of the physical system depicted in Fig. 2 even with the graphene-based SLPF.

- [1] Junichi Nakamura, *Image Sensors and Signal Processing for Digital Still Cameras* (CRC Press, Inc., New York, USA, 2005).
- [2] J. W. Goodman, *Introduction to Fourier Optics*, McGraw-Hill Physical and Quantum Electronics Series (W. H. Freeman, New York, 2005).
- [3] H. Stark and Elsevier Science & Technology (Firm), *Applications of Optical Fourier Transforms* (Academic Press, 1982).
- [4] Cynthia Goodman, The digital revolution: Art in the computer age, *Art J.* **49**, 248 (2014).
- [5] Alexandre Silva, Francesco Monticone, Giuseppe Castaldi, Vincenzo Galdi, Andrea Alù, and Nader Engheta, Performing mathematical operations with metamaterials, *Science* **343**, 160 (2014).
- [6] Daniel R. Solli and Bahram Jalali, Analog optical computing, *Nat. Photonics* **9**, 704 (2015).
- [7] Sajjad Abdollahramezani, Ata Chizari, Ali Eshaghian Dorche, Mohammad Vahid Jamali, and Jawad A Salehi,

- Dielectric metasurfaces solve differential and integro-differential equations, *Opt. Lett.* **42**, 1197 (2017).
- [8] Hossein Babashah, Zahra Kavehvash, Somayyeh Koohi, and Amin Khavasi, Integration in analog optical computing using metasurfaces revisited: Toward ideal optical integration, *J. Opt. Soc. Am. B* **34**, 1270 (2017).
- [9] Anders Pors, Michael G. Nielsen, and Sergey I. Bozhevolnyi, Analog computing using reflective plasmonic metasurfaces, *Nano Lett.* **15**, 791 (2015).
- [10] Amir Youssefi, Farzad Zangeneh-Nejad, Sajjad Abdolahramezani, and Amin Khavasi, Analog computing by brewster effect, *Opt. Lett.* **41**, 3467 (2016).
- [11] Hoyeong Kwon, Dimitrios Sounas, Andrea Cordaro, Albert Polman, and Andrea Alù, Nonlocal Metasurfaces for Optical Signal Processing, *Phys. Rev. Lett.* **121**, 173004 (2018).
- [12] Farzad Zangeneh-Nejad, Khavasi Amin, and Rejaei Behzad, Analog optical computing by half-wavelength slabs, *Opt. Commun.* **407**, 338 (2018).
- [13] Ali Momeni, Hamid Rajabipanah, Ali Abdolali, and Karim Achouri, Generalized Optical Signal Processing Based on Multioperator Metasurfaces Synthesized by Susceptibility Tensors, *Phys. Rev. Appl.* **11**, 064042 (2019).
- [14] Farzad Zangeneh-Nejad and Romain Fleury, Topological analog signal processing, *Nat. Commun.* **10**, 1 (2019).
- [15] Ali Abdolali, Ali Momeni, Hamid Rajabipanah, and Karim Achouri, Parallel integro-differential equation solving via multi-channel reciprocal bianisotropic metasurface augmented by normal susceptibilities, *New J. Phys.* **21**, 113048 (2019).
- [16] Tengfeng Zhu, Yijie Lou, Yihan Zhou, Jiahao Zhang, Junyi Huang, Yan Li, Hailu Luo, Shuangchun Wen, Shiyao Zhu, Qihuang Gong, Min Qiu, and Zhichao Ruan, Generalized Spatial Differentiation from the Spin Hall Effect of Light and Its Application in Image Processing of EDGE DETECTION, *Phys. Rev. Appl.* **11**, 034043 (2019).
- [17] Tengfeng Zhu, Yihan Zhou, Yijie Lou, Hui Ye, Min Qiu, Zhichao Ruan, and Shanhui Fan, Plasmonic computing of spatial differentiation, *Nat. Commun.* **8**, 1 (2017).
- [18] Yi Zhou, Rui Chen, Wenjie Chen, Rui-Pin Chen, and Yungui Ma, Optical analog computing devices designed by deep neural network, *Opt. Commun.* **458**, 124674 (2020).
- [19] Andrea Cordaro, Hoyeong Kwon, Dimitrios Sounas, A. Femius Koenderink, Andrea Alù, and Albert Polman, High-index dielectric metasurfaces performing mathematical operations, *Nano Lett.* **19**, 8418 (2019).
- [20] Yi Zhou, Wenhui Wu, Rui Chen, Wenjie Chen, Ruiping Chen, and Yungui Ma, Analog optical spatial differentiators based on dielectric metasurfaces, *Adv. Opt. Mater.* **8**, 1901523 (2020).
- [21] Nasim Mohammadi Estakhri, Brian Edwards, and Nader Engheta, Inverse-designed metastructures that solve equations, *Science* **363**, 1333 (2019).
- [22] T. J. Davis, F. Eftekhari, D. E. Gómez, and A. Roberts, Metasurfaces with Asymmetric Optical Transfer Functions for Optical Signal Processing, *Phys. Rev. Lett.* **123**, 013901 (2019).
- [23] Cheng Guo, Meng Xiao, Momchil Minkov, Yu Shi, and Shanhui Fan, Photonic crystal slab laplace operator for image differentiation, *Optica* **5**, 251 (2018).
- [24] Zi Wang, Tiantian Li, Anishkumar Soman, Dun Mao, Thomas Kananen, and Tingyi Gu, On-chip wavefront shaping with dielectric metasurface, *Nat. Commun.* **10**, 3547 (2019).
- [25] Parisa Karimi, Amin Khavasi, and Seyed Saleh Mousavi Khaleghi, Fundamental limit for gain and resolution in analog optical edge detection, *Opt. Express* **28**, 898 (2020).
- [26] Junxiao Zhou, Haoliang Qian, Ching-Fu Chen, Junxiang Zhao, Guangru Li, Qianyi Wu, Hailu Luo, Shuangchun Wen, and Zhaowei Liu, Optical edge detection based on high-efficiency dielectric metasurface, *Proc. Natl. Acad. Sci.* **116**, 11137 (2019).
- [27] Hamid Rajabipanah, Ali Abdolali, Shahid Iqbal, Lei Zhang, and Tie Jun Cui, arXiv:2002.06773 [physics.app-ph] (2020).
- [28] Nanfang Yu and Federico Capasso, Flat optics with designer metasurfaces, *Nat. Mater.* **13**, 139 (2014).
- [29] Nanfang Yu, Patrice Genevet, Mikhail A. Kats, Francesco Aieta, Jean-Philippe Tetienne, Federico Capasso, and Zeno Gaburro, Light propagation with phase discontinuities: Generalized laws of reflection and refraction, *Science* **334**, 333 (2011).
- [30] Shulin Sun, Kuang-Yu Yang, Chih-Ming Wang, Ta-Ko Juan, Wei Ting Chen, Chun Yen Liao, Qiong He, Shiyi Xiao, Wen-Ting Kung, Guang-Yu Guo, Lei Zhou, and Din Ping Tsai, High-efficiency broadband anomalous reflection by gradient meta-surfaces, *Nano Lett.* **12**, 6223 (2012), pMID: 23189928.
- [31] Alexander V. Kil Dishev, Alexandra Boltasseva, and Vladimir M. Shalaev, Planar photonics with metasurfaces, *Science* **339**, 1232009 (2013).
- [32] K. Achouri and O. J. F. Martin, Angular scattering properties of metasurfaces, *IEEE Trans. Antennas Propag.* **68**, 432 (2020).
- [33] Ali Momeni, Mahdi Safari, Ali Abdolali, Nazir P. Kherani, and Romain Fleury, Asymmetric Metal-Dielectric Meta-cylinders and Their Potential Applications from Engineering Scattering Patterns to Spatial Optical Signal Processing, *Phys. Rev. Appl.* **15**, 034010 (2021).
- [34] Kasra Rouhi, Hamid Rajabipanah, and Ali Abdolali, Multi-bit graphene-based bias-encoded metasurfaces for real-time terahertz wavefront shaping: From controllable orbital angular momentum generation toward arbitrary beam tailoring, *Carbon* **149**, 125 (2019).
- [35] Iqbal Shahid, Hamid Rajabipanah, Lei Zhang, Xiao Qiang, Ali Abdolali, and Tie Jun Cui, Frequency-multiplexed pure-phase microwave meta-holograms using bi-spectral 2-bit coding metasurfaces, *Nanophotonics* **9**, 703 (2020).
- [36] Mehdi Kiani, Majid Tayarani, Ali Momeni, Hamid Rajabipanah, and Ali Abdolali, Self-biased tri-state power-multiplexed digital metasurface operating at microwave frequencies, *Opt. Express* **28**, 5410 (2020).
- [37] Kasra Rouhi, Hamid Rajabipanah, and Ali Abdolali, Real-time and broadband terahertz wave scattering manipulation via polarization-insensitive conformal graphene-based coding metasurfaces, *Ann. Phys.* **530**, 1700310 (2018).
- [38] Hamid Rajabipanah, Ali Abdolali, Javad Shabanpour, Ali Momeni, and Ahmad Cheldavi, Asymmetric spatial power

- dividers using phase–amplitude metasurfaces driven by huygens principle, *ACS Omega* **4**, 14340 (2019).
- [39] Seyed Ehsan Hosseininejad, Kasra Rouhi, Mohammad Neshat, Reza Faraji-Dana, Albert Cabellos-Aparicio, Sergi Abadal, and Eduard Alarcón, Reprogrammable graphene-based metasurface mirror with adaptive focal point for THz imaging, *Sci. Rep.* **9**, 1 (2019).
- [40] Roya Kargar, Kasra Rouhi, and Ali Abdolali, Reprogrammable multifocal THz metalens based on metal–insulator transition of VO<sub>2</sub>-assisted digital metasurface, *Opt. Commun.* **462**, 125331 (2020).
- [41] Ali Momeni, Kasra Rouhi, Hamid Rajabipanah, and Ali Abdolali, An information theory-inspired strategy for design of re-programmable encrypted graphene-based coding metasurfaces at terahertz frequencies, *Sci. Rep.* **8**, 1 (2018).
- [42] Mehdi Kiani, Ali Momeni, Majid Tayarani, and Can Ding, Spatial wave control using a self-biased nonlinear metasurface at microwave frequencies, *Opt. Express* **28**, 35128 (2020).
- [43] M. Safari, A. Momeni, A. Abdolali, and N. P. Kherani, in *2019 44th International Conference on Infrared, Millimeter, and Terahertz Waves (IRMMW-THz)* (IEEE, Paris, France, 2019) p. 1.
- [44] Odysseas Tsilipakos, Thomas Koschny, and Costas M. Soukoulis, Antimatched electromagnetic metasurfaces for broadband arbitrary phase manipulation in reflection, *ACS Photonics* **5**, 1101 (2018).
- [45] Seyed Ehsan Hosseininejad, Kasra Rouhi, Mohammad Neshat, Albert Cabellos-Aparicio, Sergi Abadal, and Eduard Alarcón, Digital metasurface based on graphene: An application to beam steering in terahertz plasmonic antennas, *IEEE Trans. Nanotechnol.* **18**, 734 (2019).
- [46] Mohammad Moein Moeini, Homayoon Oraizi, and Amrollah Amini, Collimating Cylindrical Surface Leaky Waves for Highly Improved Radiation Characteristics of Holograms, *Phys. Rev. Appl.* **11**, 044006 (2019).
- [47] M. Movahhedi, M. Karimpour, and N. Komjani, Multi-beam bidirectional wideband/wide-scanning-angle holographic leaky-wave antenna, *IEEE Antennas Wirel. Propag. Lett.* **18**, 1507 (2019).
- [48] John Canny, A computational approach to edge detection, *IEEE Trans. Pattern Anal. Machine Intelligence* **PAMI-8**, 679 (1986).
- [49] D. Marr, E. Hildreth, and Sydney Brenner, Theory of edge detection, *Proc. R. Soc. Lond., B., Biol. Sci.* **207**, 187 (1980).
- [50] Ali Momeni, Hamid Rajabipanah, Mahdi Rahmazadeh, Ali Abdolali, Karim Achouri, Viktar Asadchy, and Romain Fleury, *arXiv:2012.12120* (2020).
- [51] Alexandros I. Dimitriadis, Dimitrios L. Sounas, Niko-laos V. Kantartzis, Christophe Caloz, and Theodoros D. Tsiboukis, Surface susceptibility bianisotropic matrix model for periodic metasurfaces of uniaxially mono-anisotropic scatterers under oblique TE-wave incidence, *IEEE Trans. Antennas Propag.* **60**, 5753 (2012).
- [52] Sergei Tretyakov, *Analytical Modeling in Applied Electromagnetics* (Artech House, Boston, 2003).
- [53] Karim Achouri, Guillaume Lavigne, and Christophe Caloz, Comparison of two synthesis methods for birefringent metasurfaces, *J. Appl. Phys.* **120**, 235305 (2016).
- [54] Karim Achouri and Christophe Caloz, Design, concepts and applications of electromagnetic metasurfaces, *Nanophotonics* **7**, 1095 (2017).
- [55] Achouri Karim, Bakthiar Ali Khan, Shulabh Gupta, Guillaume Lavigne, Mohamed Ahmed Salem, and Christophe Caloz, Synthesis of electromagnetic metasurfaces: Principles and illustrations, *EPJ Appl. Metamat.* **2**, 12 (2015).
- [56] G. Lavigne, K. Achouri, V. S. Asadchy, S. A. Tretyakov, and C. Caloz, Susceptibility derivation and experimental demonstration of refracting metasurfaces without spurious diffraction, *IEEE Trans. Antennas Propag.* **66**, 1321 (2018).
- [57] Edward D. Palik, *Handbook of Optical Constants of Solids* (Academic Press, 1998).
- [58] I. M. Gelfand and G. E. Shilov, *Generalized Functions. Volume 1, Properties and Operations* (AMS Chelsea Publishing, Providence, Rhode Island, 2017).
- [59] Amir Arbabi, Yu Horie, and Andrei Faraon, Dielectric metasurfaces for complete control of phase and polarization with subwavelength spatial resolution and high transmission, *Nat. Nanotechnol.* **10**, 937 (2015).
- [60] Farzad Zangeneh-Nejad and Amin Khavasi, Spatial integration by a dielectric slab and its planar graphene-based counterpart, *Opt. Lett.* **42**, 1954 (2017).